Materials & Design 253 (2025) 113939

Contents lists available at ScienceDirect

Materials & Design

journal homepage: www.elsevier.com/locate/matdes

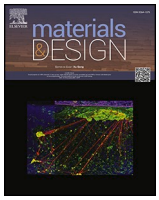

The tailored manufacturing of core (cellulose acetate)-sheath (polyvinylpyrrolidone) polymeric nanofibers for biphasic drug delivery systems using pressure-spinning

Nanang Qosim [a,b], Gareth R. Williams [c], Mohan Edirisinghe [a,*]

[a] Department of Mechanical Engineering, University College London, London WC1E 7JE, UK
[b] Department of Mechanical Engineering, Politeknik Negeri Malang, Jl. Soekarno Hatta No. 9, Malang 65141, Jawa Timur, Indonesia
[c] UCL School of Pharmacy, University College London, 29-39 Brunswick Square, London WC1N 1AX, UK

ARTICLE INFO

Keywords:
Core-sheath nanofibers
Core-sheath pressure-spinning
Non-pressure-spinnable material
Biphasic drug delivery
Polymeric fiber

ABSTRACT

Pressure-spinning is a straightforward method for manufacturing core-sheath fibers with diameters spanning from the submicrometer to micrometer scale. In this study, for the first time, a combination of cellulose acetate (CA)-polyvinylpyrrolidone (PVP) is utilized as a pressure-spun fiber matrix, despite CA having traditionally been regarded as non-pressure-spinnable. The fibers are then loaded with ibuprofen to create a biphasic drug delivery system. The resulting fibers are amorphous and cylindrical with smooth surfaces, with diameters ranging from 370 nm to 1 μm. It is observed that higher ibuprofen concentrations increase fiber diameter, while the application of higher spinning parameters has the opposite effect. *In vitro* dissolution tests reveal a dual-phase release profile, with an initial burst release due to the hydrophilic PVP sheath, followed by a sustained release phase attributed to the hydrophobic CA core. The release profile can then be tuned through fiber diameter and drug concentration adjustments. Notably, after 8 weeks of storage under ambient conditions, the fibers maintain an amorphous structure and consistent release profiles, showcasing excellent stability. These findings highlight pressure-spinning as a versatile technique for fabricating core-sheath nanofibers with customizable drug release, offering practical advantages for pharmaceutical applications in terms of enhancing therapeutic precision and patient outcomes.

1. Introduction

A search on the Web of Science using the terms “core-sheath fiber” or “core-shell fiber” as keywords reveals that within the past five years (up to December 2024), 3,064 studies have been published on this subject. This averages out to about two publications daily. This finding suggests that this topic remains highly important and continues to attract researchers’ attention. The burgeoning research interest in core-sheath fibers can be attributed to their multifaceted applications in biomedical applications such as drug delivery [1–3], tissue engineering [4–6], and wound care [7–9]. These applications offer researchers precise control over the release of drugs, the stability of the fibers, and the efficacy of combination therapies. Moreover, the increasing demand for biphasic and controlled release systems, along with advancements in fiber fabrication techniques, has driven significant research in this field.

The core-sheath structure features an inner-outer spatial arrangement that supports the creation of diverse functional materials with improved properties and performance [10]. In drug delivery applications, core-sheath fibers have several potential advantages over monolithic fibers produced by single-liquid spinning. These include the ability to deliver more complex release profiles or to avoid the initial burst of release that is frequently observed with monolithic fibers [11,12]. In our previous study [3], we employed the core-sheath pressure-spinning (CSPS) technique to produce polymeric fibers with a core-sheath structure capable of encapsulating hydrophilic or hydrophobic drugs. These fibers exhibited enhanced loading performance and achieved a more sustained release profile compared to single and blended fibers.

Another significant advantage of the core-sheath structure in fiber production, especially with electrospinning, is the ability to create fibers from solutions that are typically unspinnable on their own. This broadens the range of materials available for utilization in fiber

* Corresponding author.
E-mail address: m.edirisinghe@ucl.ac.uk (M. Edirisinghe).

https://doi.org/10.1016/j.matdes.2025.113939
Received 28 January 2025; Received in revised form 3 April 2025; Accepted 9 April 2025
Available online 12 April 2025

production [13,14]. Building on the advantages of electrospinning, we aim to produce fibers from solutions that cannot be spun by the pressure-spinning method. CSPS is a straightforward and efficient approach that has emerged as an alternative for producing micro- or nanofibers. Compared to electrospinning, CSPS operates without complex electrostatic setups, thereby reducing equipment costs. This method has specific advantages, including highly adjustable processing parameters, easily replaceable spinnerets, and a wider range of material options [15,16].

To date, CSPS has been used to process a diverse array of synthetic materials, including polyethylene oxide (PEO) [17–20], poly(methyl methacrylate) (PMMA) [17], polycaprolactone (PCL) [19,21,22], poly (lactic acid) (PLA) [19], poly(vinyl alcohol) (PVA) [19,21], and polyvinyl pyrrolidone (PVP) [18,20,22]. In a previous investigation [23], it was found that cellulose acetate (CA) was difficult to spin by pressurized gyration. This limitation was observed in both nozzle-based and orifice-based outlet systems. Additionally, electrospinning of the CA solution poses significant challenges. Natural polymers such as CA exhibit a propensity to form semi-solid material at the spinneret nozzle, even at low concentrations, which can result in needle blockages [24]. In this study, we seek to employ CA as the core layer and PVP, a spinnable material, as the sheath layer through the CSPS method to produce fibers.

CA is a naturally abundant material that offers several advantageous properties, such as renewability, favorable biocompatibility, and exceptional biodegradability. This acetate ester of cellulose has been extensively studied for a broad range of prospective applications in the form of fiber mats [25–27]. Specifically, CA-based drug-loaded fibers have been garnering increasing interest for topical and transdermal drug delivery systems [28]. PVP, on the other hand, is a hydrophilic polymer known for its excellent solubility and drug-loading capacity. It is an inert, non-toxic, biocompatible, pH-stable, and temperature-resistant polymer that facilitates the encapsulation of both hydrophilic and lipophilic pharmaceuticals. These characteristics position PVP as a highly versatile excipient in the formulation of a wide range of drug delivery systems, encompassing both traditional and advanced controlled-release formulations [25,29].

The integration of these hydrophobic and hydrophilic polymers into a core-sheath nanofiber structure allows for the creation of a biphasic drug delivery system [30]. Biphasic drug delivery systems that feature a modified drug release profile can be categorized into slow-fast and fast-slow types based on their release mechanisms. The latter represents the predominant release pattern, wherein the drug is rapidly released in the first stage, followed by a slower release in the subsequent stage. This approach has the advantage of minimizing administration frequency for patient convenience, enabling rapid therapeutic effects, and maintaining blood drug concentration over extended periods [10,31,32]. The biphasic release is currently a widely favored advanced controlled drug-release profile suitable for various therapies, including antibiotics, non-steroidal anti-inflammatory drugs, anticancer treatments, and cardiovascular therapies [33,34].

A plethora of studies have been conducted to investigate the influences of all key parameters on drug delivery system applications using conventional methods that have been widely used. CSPS, a relatively new method to manufacture core-sheath fibers, has not yet been thoroughly researched in terms of how its spinning parameters can be adjusted to control the release profile of active pharmaceutical ingredients. Additionally, we hypothesize that CSPS can enable the fabrication of CA-based core-sheath fibers, overcoming their conventional spinnability limitations. The present study aims to utilize a combination of natural and synthetic polymers to produce a family of pressure-spun fibers with tunable biphasic drug release by varying the spinning parameters, including gas pressure and rotational speed, as well as the concentration of model drugs. The simple and scalable method presented in this study is advantageous due to its ease of implementation and potential applicability in an industrial context.

2. Experimental

2.1. Materials

PVP (Mw 1,300,000 g mol^{-1}), CA (39.8 % acetyl, Mw 30,000 g mol^{-1}), ibuprofen (IBP; Mw 206.28 g mol^{-1}), phosphate-buffered saline (PBS; pH 7.4), acriflavine hydrochloride, rhodamine B, and acetone ($\geq$ 99.5 %) were purchased from Sigma-Aldrich (Gillingham, UK). Ethanol absolute and dimethylformamide (DMF, $\geq$ 98 %) were obtained from VWR Chemicals (Strasbourg, France). All materials were of analytical grade and used without further purification.

2.2. Preparation of polymeric solutions

Polymeric solutions were prepared by first dissolving 1.5 g of PVP and CA separately in 15 mL of ethanol and a mixture of acetone:distilled water (5:1, v/v), respectively. The solutions were subsequently stirred using an MS7-H550-Pro magnetic stirrer (DLAB, Beijing, China) at a rotational speed of 260 RPM for 24 h until a homogeneous solution was obtained. Subsequently, IBP at concentrations of 2.5 %, 5 %, and 7.5 %, as specified in Table 1, was then added to each solution and stirred for an additional 24 h.

2.3. Solution characterization

All prepared solutions were thoroughly analyzed for their surface tension and viscosity using specific instruments: Tensiometer K9 (Kruss GmbH, Hamburg, Germany) and DV-III Ultra programmed rheometer (Brookfield Engineering Laboratories Inc., Massachusetts, USA), respectively. The Wilhelmy plate technique was used to measure the surface tension. All measurements were performed in triplicate, with the results averaged and expressed as the mean $\pm$ standard deviation (SD). The detailed results, including specific values for surface tension and viscosity for each solution, are summarized in Table 1.

2.4. Fabrication of core-sheath pressure-spun nanofibers

Fig. 1a provides a detailed illustration of the CSPS method, highlighting the key components in the process. The CSPS vessel or pot, as shown in Fig. 1b, consists of two distinct compartments: the core and the sheath reservoirs. The vessel is constructed from aluminum and features four coaxial nozzles as the outlet system, with inner diameters of 0.65 mm (core) and 2.2 mm (sheath). The spinning process started by filling the pot with the polymeric solution. The polymeric solution was initially mixed for 5 min using a DAC 150.1 FVZ-K speed mixer (Hauschild, Germany). Subsequently, 4 mL of CA and PVP solutions were loaded into the core and sheath reservoirs, respectively.

The tailored production of core-sheath nanofibers was investigated by varying the spinning parameters, including the rotational speed and gas pressure, as detailed in Table 2. The gas pressure ranging from 0.1 to 0.3 MPa was introduced into the spinning vessel via a gas inlet. In this method, the gas pressure plays a crucial role in increasing the kinetic energy of polymer jets, facilitating the formation of finer fibers by overcoming surface tension and viscosity. In comparison to centrifugal spinning or rotary jet spinning without pressure, the pressure provided

Table 1
Details of the solution properties of CA and PVP investigated in this work.

Drug concentration (% w/v)	Solutions	Viscosity (mPa s)	Surface tension (mN m^{-1})
2.5	CA	500 $\pm$ 12	33.4 $\pm$ 0.2
	PVP	460 $\pm$ 11	23.3 $\pm$ 0.2
5	CA	580 $\pm$ 13	34.6 $\pm$ 0.6
	PVP	540 $\pm$ 11	26.5 $\pm$ 0.8
7.5	CA	660 $\pm$ 10	34.5 $\pm$ 0.8
	PVP	620 $\pm$ 10	26.7 $\pm$ 0.1

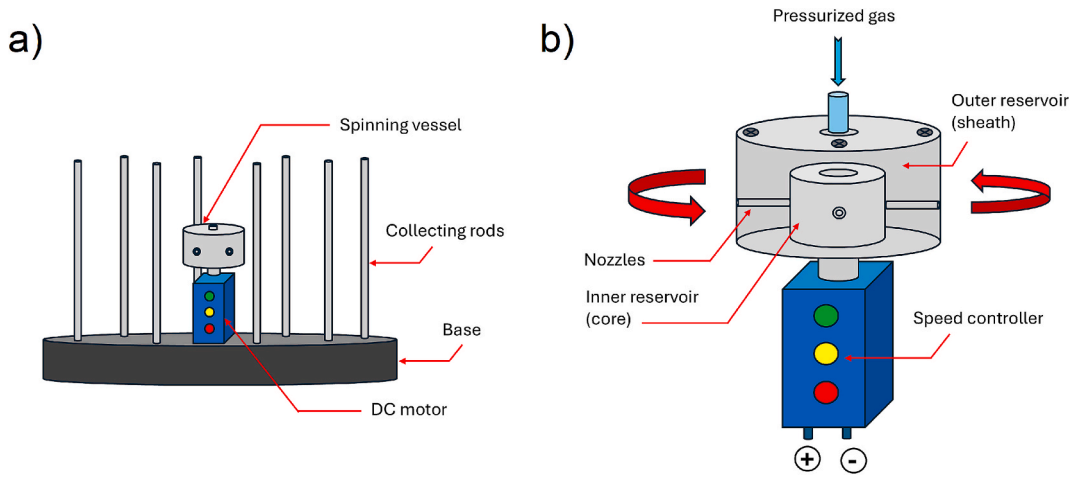

Fig. 1. A) illustration of the CSPS setup; b) details of the spinning vessel.

Table 2
Optimization parameters for CA/PVP nanofiber synthesis.

Label	Drug concentration (% w/v)	Spinning parameters	
		Gas pressure (MPa)	Rotational speed (RPM)
F1	2.5	0.2	25,000
F2	5	0.2	25,000
F3	7.5	0.2	25,000
F4	5	0.1	25,000
F5	5	0.3	25,000
F6	5	0.2	12,000
F7	5	0.2	32,000

by CSPS enhances the acceleration of the spinning flow [16]. The rotating vessel was simultaneously driven by a DC motor (Dremel 3000, Breda, Netherlands) at a speed ranging from 12,000 to 32,000 RPM. During the spinning process, materials from both compartments were simultaneously extruded under pressure, enabling the formation of nanofibers with a core-sheath configuration. The fibers ejected from the nozzles were collected on stainless steel rods positioned 100 mm from the nozzle ejection point. The fiber fabrication continued for 30 s under ambient conditions (21.0–21.5 °C and 43–44 % relative humidity).

2.5. Fiber characterization

2.5.1. Scanning electron microscopy

The morphology of the produced nanofibers was observed using a scanning electron microscope (SEM; GeminiSEM 360, Carl Zeiss, Oberkochen, Germany) operated at an excitation voltage of 1 kV. A Java-based image processing software, ImageJ (developed by the National Institutes of Health, Bethesda, MD, USA), was used to measure the fiber dimensions quantitatively. This program measures the diameters of 100 individual fiber strands observed in the SEM images, enabling the calculation of the average fiber diameter and size distribution. The data obtained were presented as the mean ± SD and then graphically represented using Origin Pro software. Additionally, the uniformity of the fibers was evaluated using the coefficient of variation (CV). Fibers with CV less than 0.3 were considered uniform [35].

2.5.2. Confocal microscopy

Confocal microscopy (LSM 710, Carl Zeiss, Oberkochen, Germany), equipped with a 25 mW argon ion laser, was used to observe the internal structure of the nanofiber produced. The sample preparation involved the incorporation of 4 mg of rhodamine B into the sheath solution, while 4 mg of acriflavine hydrochloride was added to the core solution to enable fluorescent visualization of the distinct layers. The confocal images captured were then processed and analyzed using ZEN Microscopy Software.

2.5.3. Optical microscopy

In addition to employing the confocal microscopy method, a VHX-7000 optical microscope (Keyence Ltd., Milton Keynes, UK) was also used to observe the internal structure of the manufactured fibers. Optical microscopy images were captured under full coaxial illumination at a magnification of 1000x. To aid the examination of the fibers' internal structure using this method, fibers were produced with the addition of rhodamine B into the CA solution. This increased the contrast between the core and sheath layers on the fibers.

2.5.4. X-ray diffraction

X-ray diffraction (XRD) analysis was conducted on both the raw polymers/drug and nanofiber samples using a Rigaku MiniFlex 600 diffractometer system (Rigaku, Tokyo, Japan), equipped with a Cu-Kα radiation source that operates at a wavelength of 1.5418 Å. For measurement, all samples were mounted on aluminum specimen holders. The XRD patterns were recorded over a 2θ range of 3° to 40°. The instrument was set to a step size of 0.02° while the scan rate was maintained at 5.0° per minute.

2.5.5. Differential scanning calorimetry

Differential scanning calorimetry (DSC) analysis was performed with a STAR^e System DSC 3 (Mettler Toledo, Ohio, USA). For each test, ~5 mg of the material or fiber sample was placed and sealed in an aluminum pan. A second empty aluminum pan, serving as a reference, was also prepared. Both the sample pan and the reference pan were positioned in the DSC sample holder for analysis. The thermal scanning procedure involved heating the samples from 0 to 300 °C at a constant rate of 10 °C min^{-1}. During the entire measurement process, the DSC instrument was purged with a continuous flow of nitrogen gas at a rate of 50 mL min^{-1}.

2.5.6. Fourier transform infrared spectroscopy

Spectral data were collected for the model drug, the polymers, and the drug-loaded core-sheath nanofibers using a Nicolet iS50 spectrometer (Thermo Scientific, Massachusetts, USA). To conduct the analysis, each sample was placed onto the attenuated total reflectance (ATR) crystal of the spectrometer, ensuring proper contact for optimal signal detection. The samples were examined over 10 rounds using the OMNIC Spectra software. The spectral range for the analysis spanned from 4000 cm^{-1} to 500 cm^{-1}, and a resolution of 4 cm^{-1} was maintained throughout the procedure to ensure spectral data with well-defined peaks.

2.6. Estimation of core diameter and sheath thickness

Given the established unspinnability of CA with the pressure-spinning method, a direct comparison of the diameter of monolithic fibers with that of core-sheath fibers was precluded. The estimation of core diameter and sheath thickness was thus performed by removing the sheath layer from the fibers, leaving only the core. ~100 mg of fiber samples were soaked in distilled water for 5 min. Distilled water was chosen as the medium due to its ability to dissolve PVP quickly without affecting CA. The samples were then dried and further observed using SEM (Section 2.5.1) to calculate the average fiber diameter. The thickness of the sheath layer was estimated by comparing the aggregate fiber diameter prior to and following the removal of the sheath layer.

2.7. Drug loading

To determine the amount of IBP loaded in the fiber samples, 10 mg of IBP-loaded nanofibers were weighed and immersed in 10 mL of DMF for 24 h to ensure complete dissolution of all materials. Subsequent to the stirring process, 3 mL of samples were taken out of the solutions for analysis. These samples were then analyzed using a Jenway 7315 UV spectrophotometer (Cole-Parmer Ltd., St. Neots, UK), set at a maximum absorption wavelength of $\lambda_{max} = 267$ nm, corresponding to IBP detection. The IBP concentration in each sample was determined by referencing a previously established calibration curve for IBP dissolved in DMF. Once the concentrations were obtained, the encapsulation efficiency (EE%) of the nanofibers was calculated using a predefined equation (Eq. (1). This equation quantifies the amount of IBP successfully encapsulated relative to the initial loading. The entire set of experiments was conducted in triplicate.

$$EE\% = \frac{\text{actual drug loading}}{\text{theoretical drug loading}} \text{ x } 100\% \quad (1)$$

2.8. Dissolution test

The dissolution test was conducted by immersing 15 mg of IBP-loaded nanofibers into 15 mL of PBS, which served as the test medium. The setup was then incubated at a constant temperature of 37 °C to simulate physiological conditions. At predetermined time intervals ranging from 0 to 12 h, 3 mL aliquots of the solution were withdrawn to monitor the release of IBP from the nanofibers. Each time an aliquot was removed, it was replaced with an equal volume of fresh PBS to maintain sink conditions throughout the experiment. The UV spectrophotometer was then used to measure the absorbance of each filtered aliquot at a wavelength of $\lambda_{max} = 267$ nm. All dissolution studies were performed under sink conditions. The test was conducted in triplicate for each formulation, and the data obtained were reported as mean values ± SD. The drug release profiles, representing the cumulative percentage of IBP released over time, were plotted to provide a visualization of the release kinetics of the drug from the nanofibers over the 12-h testing period.

2.9. Stability studies

The IBP-loaded nanofibers were stored under ambient conditions (19–21 °C, relative humidity 30–40 %) for a period of 8 weeks, allowing them to age naturally. After this aging period, the nanofibers were subjected to a detailed characterization process in order to assess any changes in their physical or chemical properties. DSC and XRD analyses were conducted in accordance with the protocols outlined in Sections 2.5.5 and 2.5.4, respectively, to evaluate their thermal behavior and crystallinity. In addition to these characterizations, the *in vitro* drug release study, as described in Section 2.6, was repeated to assess whether the aging process had influenced the release profile of IBP from the nanofibers. The drug release experiments were performed in triplicate and compared with the release behavior observed prior to aging.

2.10. Statistical analysis

Statistical differences between groups were evaluated using one-way ANOVA, followed by Tukey's HSD (honestly significant difference) post hoc test. The IBM SPSS 29 software (IBM, USA) was utilized for the analysis, with a significance threshold set at $p < 0.05$, ensuring a confidence level above 95 % [36].

3. Results and discussion

3.1. Morphology and size distribution

For the first time, a non-pressure-spinnable natural polymer, CA, in combination with the synthetic polymer PVP, was successfully fabricated into core-sheath fibers using the CSPS method. As depicted in Fig. 2, the combination of CA (core) and PVP (sheath) produced cylindrical fibers with smooth surfaces. Samples F4 and F7 exhibited CV values of 0.28 and 0.27, respectively, indicating uniformity. In contrast, samples F1, F2, F3, F5, and F6 exhibited CV values of 0.50, 0.39, 0.53, 0.43, and 0.40, respectively, indicating less uniform fibers. The core-sheath fibers produced exhibited a lack of uniformity, attributable to the high loading of the model drug. While one of the key advantages of CSPS is its ability to accommodate high drug-loading capacities, excessive IBP content led to less uniform fibers being formed.

Moreover, the employment of a lighter aluminum spinning vessel and smaller nozzle sizes facilitated the production of core-sheath fibers in the nanometer range. In comparison, previous studies (summarized in Table 3) reported that stainless-steel spinning vessels produced core-sheath pressure-spun fibers in the micrometer range. As shown in Table 3, the rotational speed of stainless-steel vessels was limited to 6,000–8,500 RPM. In contrast, in this study, the use of an aluminum vessel allowed for a significantly higher rotational speed of up to 32,000 RPM, enabling the fabrication of nanometer-scale fibers.

3.1.1. Effect of drug concentration on nanofiber diameter

The histogram plots (Fig. 2) show the effect of IBP concentration on nanofiber diameter. The data indicates that an increase in the diameter of the nanofibers produced is associated with an increase in the model drug concentration in the solution. Incorporating 2.5 % of IBP into the solutions resulted in nanofibers with a diameter of 380 nm (F1). In formulations F2 and F3, increasing the model drug concentration to 5 % and 7.5 %, respectively, produced nanofibers with larger diameters, 480 nm and 850 nm. Statistical tests confirmed that the average diameters of all groups were significantly different ($p < 0.05$). The observed increase in nanofiber diameter was expected due to the higher IBP concentration, which led to an increase in solution viscosity (Table 1). Viscosity, in addition to surface tension, is a pivotal solution property that influences nanofiber diameter in the pressure-spinning fabrication process. The rise in solution viscosity dispenses a greater mass of solute per unit of time and generates more resistance to centrifugal force and dynamic fluid blowing while concurrently hindering solvent evaporation [37]. This phenomenon has been reported in several studies, which have shown that pressure-spun fiber diameter increases with higher solution concentration [18,23,38].

3.1.2. Effect of spinning parameters on nanofiber diameter

In the pressure-spinning method, gas pressure and rotational speed are the two primary parameters. Fig. 2 also depicts the scanning electron micrographs of nanofibers produced at a constant rotational speed (25,000 RPM) and at varying gas pressures (0.1, 0.2, and 0.3 MPa). The nanofibers obtained by applying different gas pressures were characterized by continuity, smoothness, and the absence of beads. Additionally, the absence of visible pores on the nanofibers' surface was observed. The produced nanofibers exhibited a size distribution that followed a unimodal normal distribution, characterized by a single peak and a broad spread. For nanofibers generated with 0.1 MPa of gas

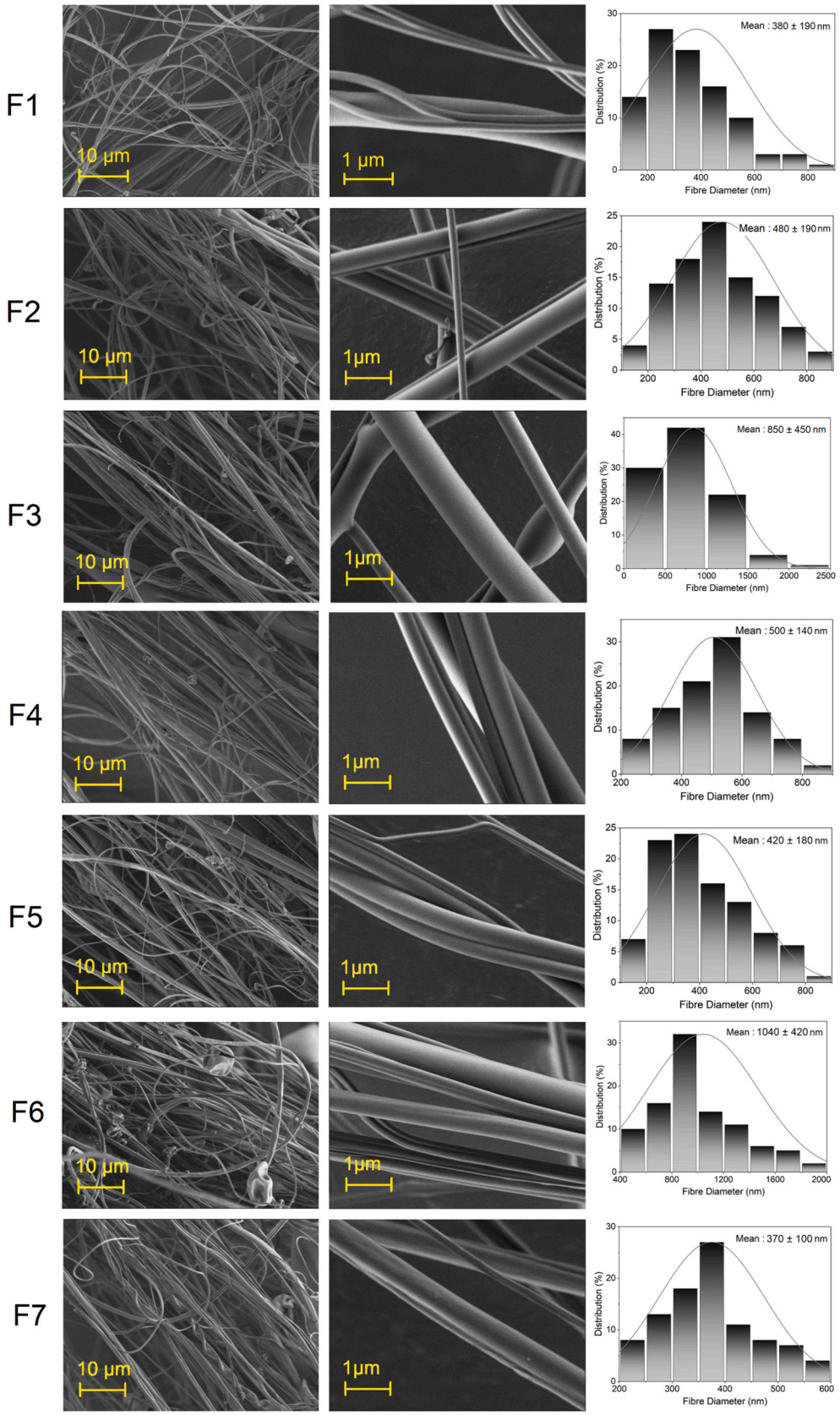

Fig. 2. Scanning electron micrographs of all CA/PVP core-sheath samples along with their size distributions.

Table 3
Core-sheath fibers manufactured by CSPS with stainless-steel pot and their diameters.

Raw material and solvent Core polymer (solvent)	Sheath polymer (solvent)	Rotational speed (RPM)	Diameter of nozzle (outer:inner) (mm)	Fiber diameter (μm)	Ref.
PEO (water)	PMMA (chloroform)	8,000	1.6:0.8	27	[17]
PMMA (chloroform)	PEO (water)			33	
PMMA (chloroform)	PMMA (chloroform)			37	
PCL (chloroform)	PVA + hydroxyapatite (water)	6,000	2:1	3 to 4	[21]
PVP + tetracycline hydrochloride (ethanol)	PCL (chloroform)	8,000	1.6:0.8	4 to 5	[22]
PVP (ethanol)	Ethyl cellulose (ethanol)	8,500	2.2:0.85	2 to 3	[3]
PCL (chloroform)	PEO + garlic (chloroform)	6,000	1.6:0.8	1 to 3	[20]

pressure (F4), the average diameter was measured to be 500 nm, with a ± SD of 140 nm. However, the application of higher gas pressures, specifically 0.2 and 0.3 MPa, resulted in nanofibers with a reduced mean diameter, measuring 480 nm (F2) and 420 nm (F5), respectively. A statistical analysis revealed that the average diameters of F2 and F4 were not significantly different ($p > 0.05$). However, a statistically significant difference ($p < 0.05$) was observed between F2 and F5, as well as between F4 and F5. Overall, the mean nanofiber diameter tended to decrease as the gas pressure increased at a constant rotational speed.

The application of a higher gas pressure has been demonstrated to enhance the combined shearing forces of centrifugal force and blowing. This enhanced effect counteracts surface tension, causing polymer jets to elongate. The result is a reduction in jet diameter at the nozzle of the vessel, thereby promoting the formation of thinner nanofibers. The mechanism underpinning this effect involves the increased pressure, which has been shown to boost the kinetic energy of the spinning jets. This, in turn, aids in their further elongation during the stretching phase [16,37]. Furthermore, the blowing process enhances solvent evaporation by increasing the relative speed of the gas flow at the liquid–air interface of the polymer drops at the nozzles. This facilitates solvent diffusion to the surface of the polymer drops and further contributes to fiber thinning [18,39].

The application of varying rotational speeds had a significant impact on the morphology and diameter of the core-sheath nanofibers produced. SEM micrographs of nanofibers manufactured at a constant medium gas pressure of 0.2 MPa and different spinning RPMs (F2, F6, and F7) are depicted in Fig. 2. A low spinning speed (12,000 RPM) produced nanofibers with a diameter of 1040 nm, with a ± SD of 420 nm. A higher magnification image reveals the presence of beads, which are indicative of insufficient solvent evaporation and jet elongation. It is imperative to maintain a balance between the gas flow rate and the liquid flow rate to ensure the production of smooth, bead-free fibers [40].

Increasing the rotational speed to a higher level, 25,000 RPM, could reduce the diameter of the nanofibers produced to 480 nm (F2). The nanofiber with the smallest diameter (370 nm) was obtained by applying the highest rotational speed of 32,000 RPM (F7). Statistically, F6 was significantly different from both F2 and F7 ($p < 0.05$), whereas F2 and F7 were not significantly different ($p > 0.05$). As the rotational speed increases, the centrifugal force strengthens, thereby enabling more substantial manipulation of the polymer solution [41]. The histograms in Fig. 2 illustrate unimodal fiber size distributions for all the nanofibers produced.

3.2. Confocal microscopy observation

Fig. 3 shows the presence of a core-sheath structure in the fibers observed. Two channels were utilized in this characterization by confocal microscopy. The first channel was designed to identify the presence of CA, as indicated by the green fluorescence emitted by acriflavine hydrochloride. The second channel was configured to identify the presence of PVP, which exhibited a red hue emitted by rhodamine B. Overall, the confocal microscopy images confirmed the presence of a core-sheath structure in all the samples analyzed. In Channel 1, the green fluorescence indicating the CA core is clearly visible, while in Channel 2, the red fluorescence corresponding to the PVP sheath is detected. The fluorescent area observed in Channel 2 appears to be narrower in comparison to the broader fluorescent region detected in Channel 1. When the images from both channels are merged, it becomes evident that the red zone, representing the PVP sheath, completely encompasses the green zone of the CA core, which turns yellow.

This finding proves that the CSPS method effectively produces nanofibers with a well-defined core-sheath architecture using a combination of natural CA and synthetic PVP. The results indicate that the core-sheath structure is consistently achieved, irrespective of the spinning parameters employed or the drug concentration incorporated into the fibers. This consistency underscores the versatility and reliability of the CSPS method in fabricating nanofibers with a well-defined core-sheath structure, highlighting its potential for applications in drug delivery systems.

3.3. Optical microscopy observation

The images captured from the optical microscope, as depicted in Fig. 4, provide further evidence that the produced nanofibers exhibit a distinct core-sheath structure. Staining the core solution with a fluorescent dye enabled the selective visualization of the core within the nanofibers, as indicated by a darker region, thereby generating a clear contrast against the surrounding sheath. Moreover, this method enabled the quantitative measurement of fiber dimensions, which is presented in Table 4. This observation unequivocally confirms the presence of core-sheath structures across all examined samples, underscoring the consistency of this feature in the fabricated nanofibers.

3.4. Estimation of core diameter and sheath thickness

Despite the feasibility of observing and measuring the sheath layer thickness with an optical microscope (Fig. 4), the obtained results were inadequate for determining the core diameter and sheath layer thickness of the resulting fibers. This limitation could be attributed to the limited number of samples observed and the inability to discern the sheath layer thickness of fibers with smaller diameters using an optical microscope. Consequently, the approach adopted in this study involved the removal of the sheath layer. To ensure that after immersion, there was no PVP (sheath layer) remaining on the samples, the soaked samples were tested by FTIR, and the results are shown in Fig. S1. The spectra of all samples after immersion show that the samples only contain CA with typical peaks at 1735, 1367, 1216, and 1032 cm^{-1}. A similar approach was successfully implemented by Gu et al. [42], in which they managed to estimate the core-to-sheath ratio of core (PVA)-sheath (poly(L-lactic acid), PLLA) fibers by removing the PLLA sheath using chloroform.

Fig. 5 depicts SEM micrographs of the sample after the sheath layer was removed. It can be seen that the CA fibers exhibit a cylindrical shape with a smooth surface. The comparison of the core diameter and the layer thickness is shown in Table 5. The samples F1 and F6 had CV of 0.27, while F2 and F5 had CV of 0.30, indicating their uniformity. Conversely, samples F3, F4, and F7 exhibited CV values of 0.32, 0.41, and 0.33, respectively, indicating the fibers were less uniform. The

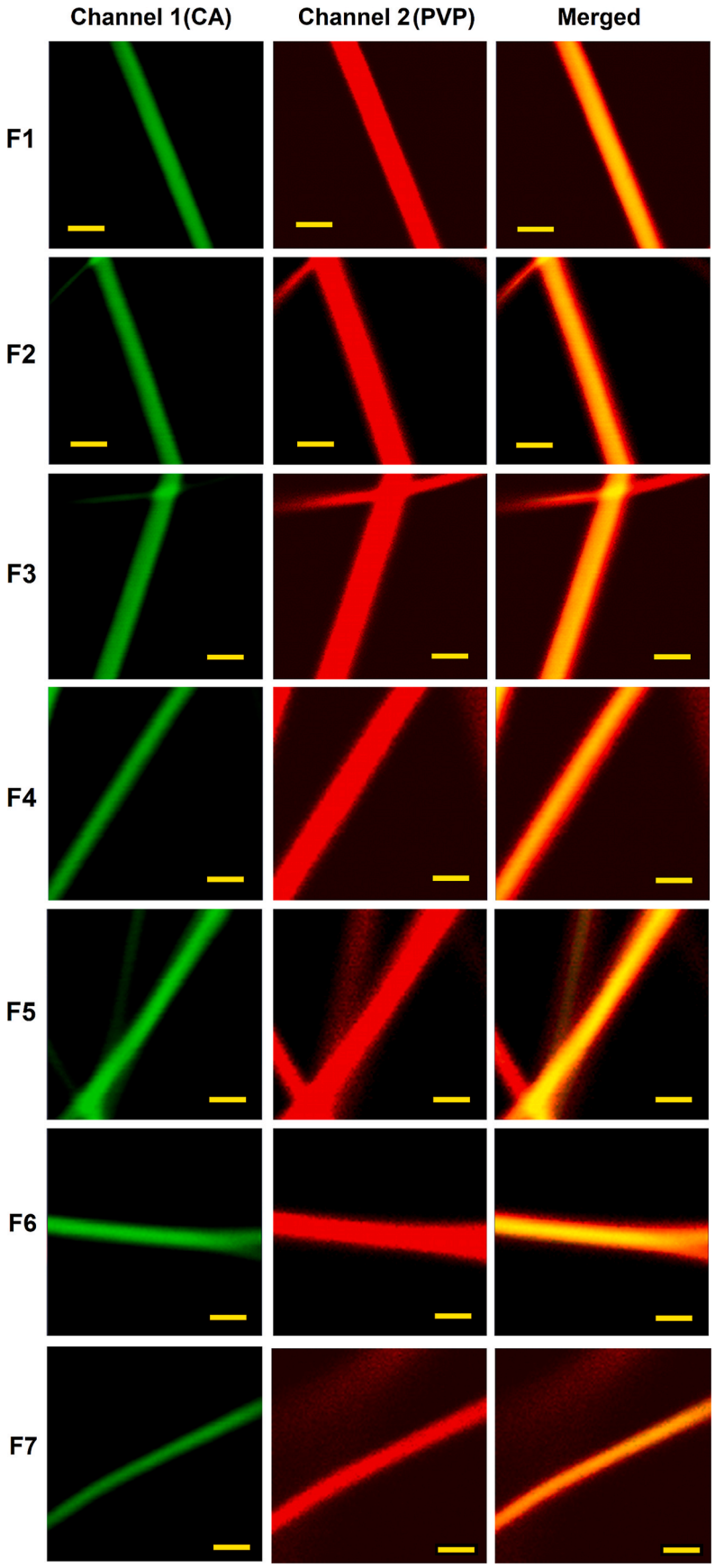

Fig. 3. Confocal microscopy images of CA/PVP core-sheath nanofibers (scale bars represent 2 μm).

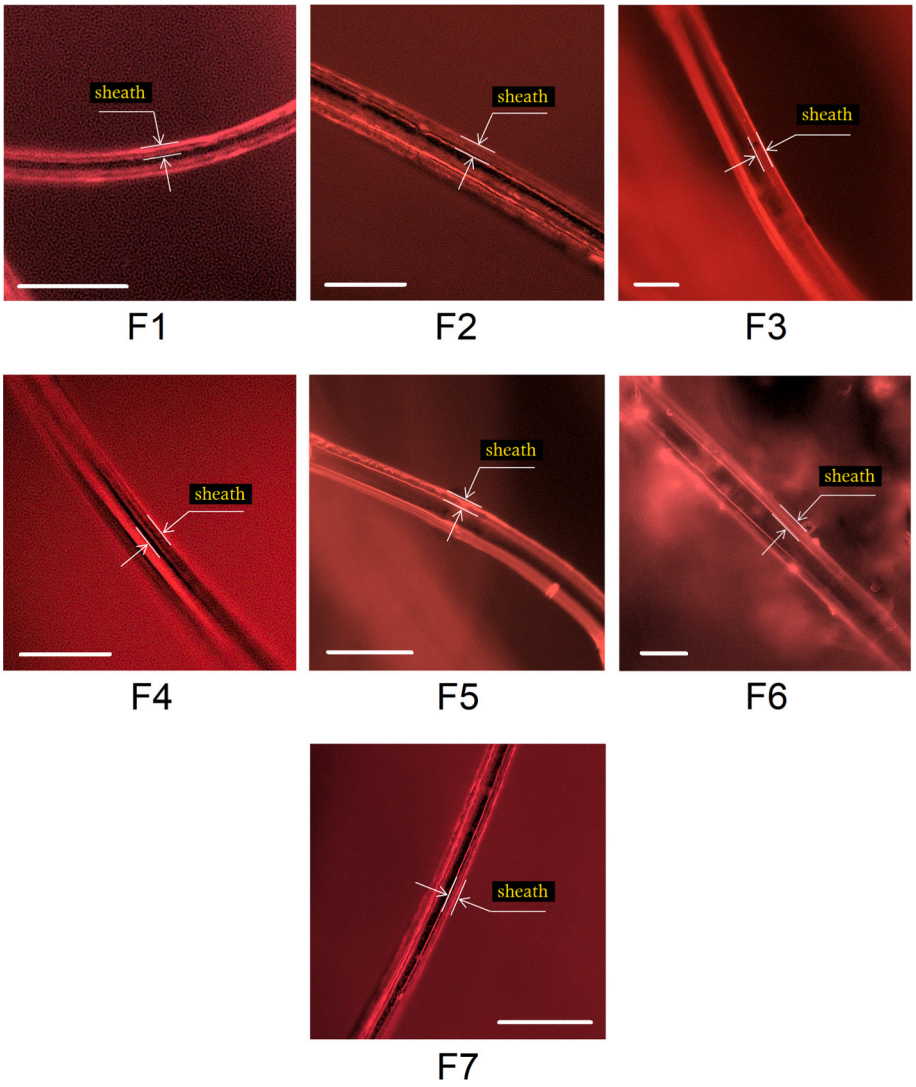

Fig. 4. Images of CA/PVP core-sheath structure captured by a high-accuracy digital microscope (scale bars represent 1 μm).

Table 4
Quantitative measurement of fiber dimensions using a high-accuracy digital microscope.

Sample	Diameter of core-sheath fibers (nm)	Diameter of core (nm)	Thickness of sheath layer (nm)
F1	310	70	120
F2	590	250	170
F3	760	360	200
F4	500	140	180
F5	470	230	120
F6	950	410	270
F7	360	140	110

removal of the sheath layer has been observed to enhance the uniformity of the fibers. This phenomenon can be attributed to the fact that the removal process also eroded the beads on the fiber and dissolved imperfect fibers when forming the core-sheath structure, resulting in more uniform fibers.

As expected, the diameter of the core and the thickness of the sheath layer in the nanofibers produced were also influenced by the spinning parameters. The core diameters of the nanofibers produced at a constant medium gas pressure of 0.2 MPa with different rotational speeds of 12,000, 25,000, and 36,000 RPM were 340 nm (F4), 300 nm (F2), and 260 nm (F5), respectively. A non-significant difference was observed between F4 and F2 ($p > 0.05$). Maintaining the rotational speed at 25,000 RPM and varying the working pressure from 0.1 to 0.3 MPa resulted in the generation of nanofibers with a core average diameter of 660 nm (F6) and 240 nm (F7), respectively. The statistical analysis revealed that F6 was significantly different from both F2 and F7 ($p < 0.05$), while F2 and F7 showed no significant difference ($p > 0.05$). The diameter of the core and the thickness of the sheath layer tend to decrease as the spinning speed or gas pressure increases. Higher spinning speeds generate greater centrifugal forces, which stretch and thin the fibers, leading to a reduction in both the core diameter and sheath thickness. Furthermore, an increase in gas pressure has been shown to enhance fiber elongation by exerting higher aerodynamic drag, thereby leading to further thinning of both the core and sheath layers [16,41].

Furthermore, the concentration of IBP, which enhanced the viscosity of the resulting solution, also influenced the diameter of the core and the thickness of the sheath layer. As shown in Table 5, the formulation with the lowest drug concentration (F1) generated nanofibers with a core average diameter of 260 nm. However, increasing the IBP concentration to 5 % and 7.5 % resulted in an increase of the core diameter to 300 nm and 500 nm, respectively. All sample groups were significantly different from each other ($p < 0.05$). As previously discussed, an increase in the model drug concentration means more material is being incorporated into the solution. This, in turn, raises the solution's viscosity, thereby reducing its ability to undergo stretching under centrifugal and

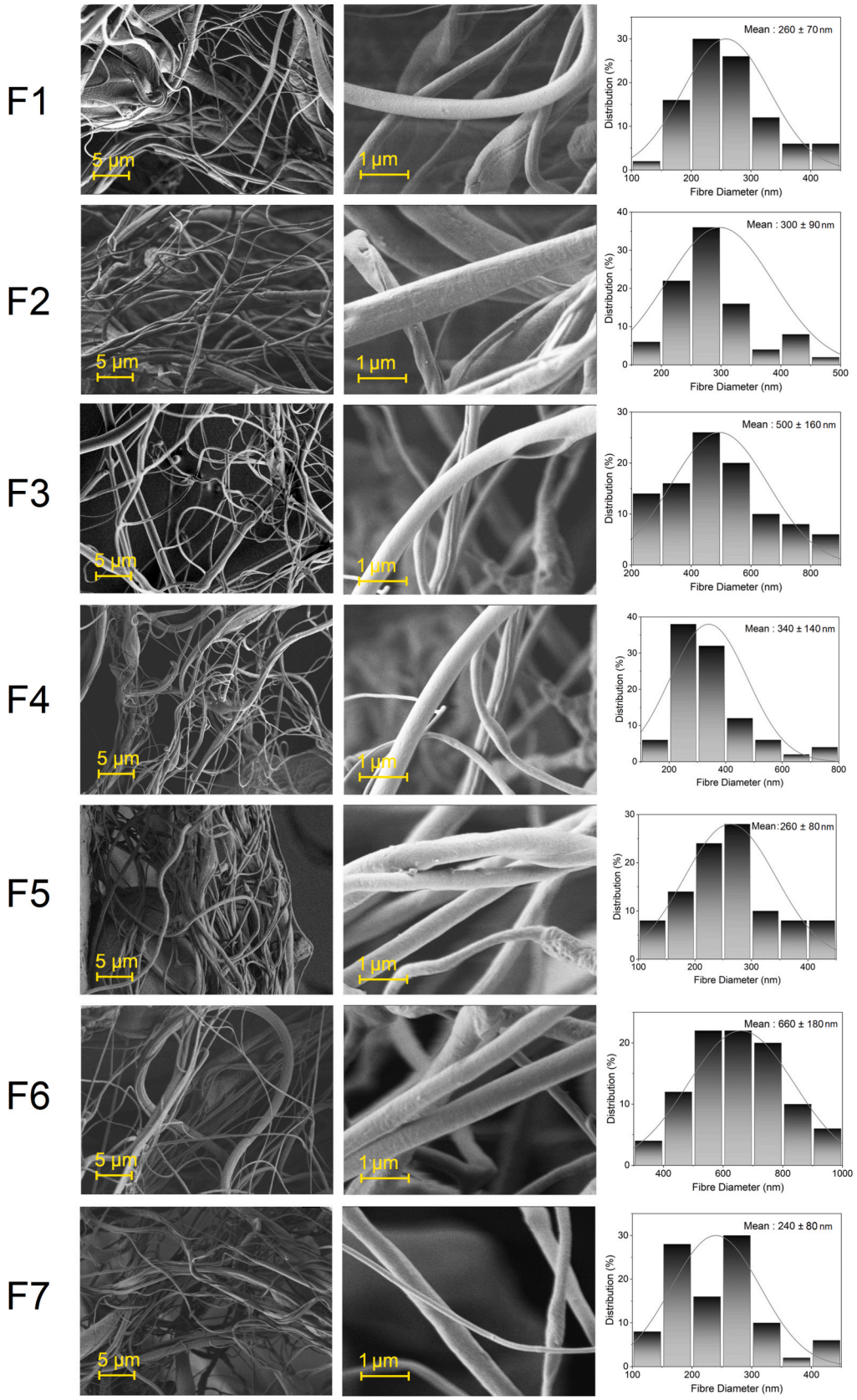

Fig. 5. Scanning electron micrographs of samples after sheath layer removal together with their size distributions.

Table 5
Diameter of samples before and after sheath layer removal.

Sample	Diameter of core-sheath fibers (nm)	Diameter of core (nm)	Estimated thickness of sheath layer (nm)
F1	380 ± 190	260 ± 70	~120
F2	480 ± 190	300 ± 90	~180
F3	850 ± 450	500 ± 160	~350
F4	500 ± 140	340 ± 140	~160
F5	420 ± 180	260 ± 80	~160
F6	1,040 ± 420	660 ± 180	~380
F7	370 ± 100	240 ± 80	~130

aerodynamic forces. Consequently, this results in the formation of thicker fibers.

3.5. X-ray diffraction

XRD analyses were performed to test the physical form of the fiber samples. The results obtained are plotted in Fig. 6. As depicted in Fig. 6a, the XRD pattern of IBP exhibited strong Bragg reflections at 6.1°, 12.2°, 16.6°, 17.8°, 19.1°, 22.3°, and 27.8°, indicating its crystalline nature [24]. Conversely, the diffraction patterns of CA and PVP exhibited an absence of Bragg reflections, suggesting their amorphous nature [25,28].

Fig. 6b depicts the XRD patterns of the IBP-loaded nanofibers. Overall, the fibers lacked Bragg reflections in their patterns, instead displaying broad haloes, indicating they consisted of amorphous solid dispersions. Consequently, it could be assumed that the drug was dispersed in the nanofibers in an amorphous state, a phenomenon that is frequently observed in pressure-spun systems due to the rapid drying process. The fast evaporation process inhibits the production of highly-ordered crystallites, resulting in the model drug existing in an amorphous state [43].

3.6. Differential scanning calorimetry

Fig. 7 displays the DSC thermograms of raw materials and IBP-loaded nanofibers. The DSC thermogram of pristine IBP displayed a single endothermic peak, which is a characteristic of its melting point of 77 °C. The DSC trace of PVP was expected to manifest an amorphous form, as confirmed by the XRD results discussed in Section 3.5. However, an endothermic peak was observed at 190 °C, which was also observed in all the fibers produced despite their amorphous nature, as verified by XRD analysis. This phenomenon is attributed to a relaxation endotherm superimposed on and obscuring the glass transition [44].

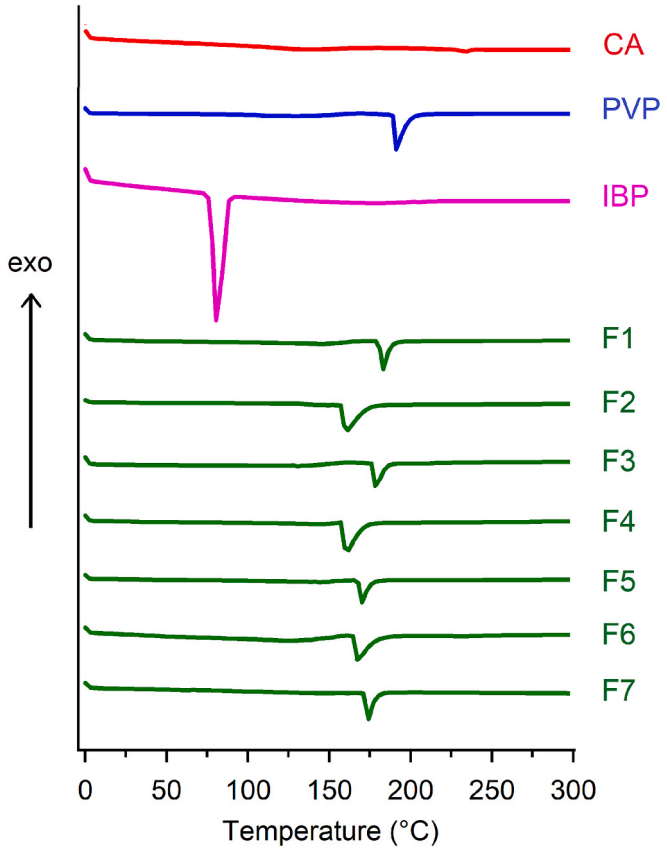

Fig. 7. DSC thermograms of raw materials and IBP-loaded nanofibers.

In the DSC thermograms of all IBP-loaded nanofibers, the characteristic melting endotherm of IBP was absent, indicating that IBP was no longer in a crystalline form and had transitioned into an amorphous state in the pressure-spun nanofibers. The fast evaporation of solvent during the spinning likely contributed to the production of amorphous materials [45]. The findings from XRD and DSC unequivocally demonstrated that IBP was extensively dispersed inside the core-sheath nanofiber matrix and existed in an amorphous state, resulting in the loss of the original structure of the pure materials.

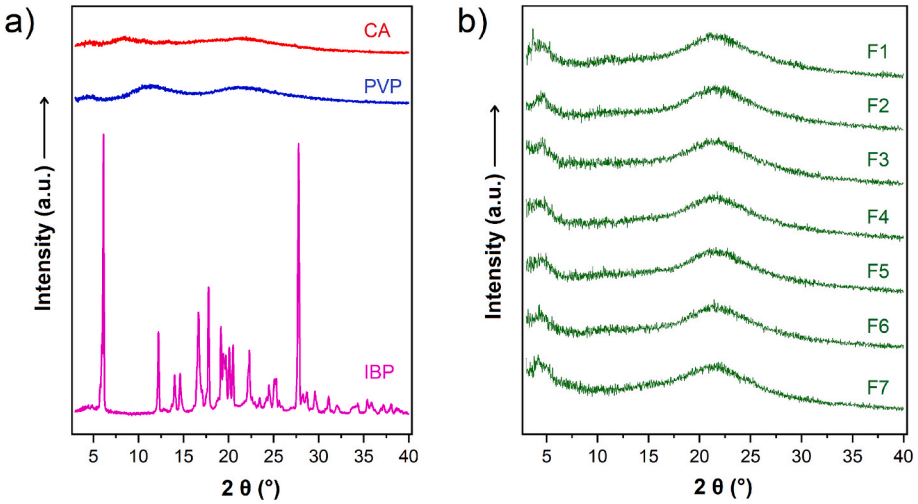

Fig. 6. XRD pattern of a) raw materials; b) IBP-loaded nanofibers.

3.7. Infrared spectroscopy

The FTIR spectra demonstrated compatibility between the materials. As shown in Fig. 8, the spectrum of PVP displayed several characteristic peaks that correspond to its molecular vibrations. A prominent peak around 1652 cm^{-1} indicated the stretching of the C=O (carbonyl) bond in the pyrrolidone ring. Additionally, a peak at 1422 cm^{-1} represented C-H bending vibrations, while another peak at 1282 cm^{-1} was associated with CH_2 wagging vibrations [3,25]. The FTIR spectrum of CA exhibited key features, including a strong peak at 1735 cm^{-1}, which corresponds to the C=O stretching vibrations of the acetyl group, while another significant peak at 1032 cm^{-1} was associated with C–O–C stretching vibrations typical of the ether linkages in cellulose. Additionally, peaks observed at 1367 cm^{-1} and 1216 cm^{-1} were related to C–H bending and C–O stretching, respectively [25,46,47].

A comparison of the spectrum of nanofibers indicated that the core–shell materials exhibited some typical peaks of PVP and CA, thereby confirming the existence of the components in the nanofibers. The alterations in the C=O region were attributed to the interactions between PVP and CA molecules [43]. The IBP spectra exhibited a distinctive peak at 1720 cm^{-1}, indicative of the stretching vibrations of its singular C=O groups. However, in the spectra of IBP-loaded fibers, this peak subsequently merged with the C=O bands of the PVP and CA, which is indicative of hydrogen bonding.

3.8. Drug loading

The EE% for core-sheath nanofibers is given in Table 6. Previous studies have demonstrated that core-sheath pressure-spun fibers, composed of PVP and ethyl cellulose polymers, were able to encapsulate IBP with up to 83 % efficiency [3]. In the present study, the system developed along with the varying spinning parameters was able to increase the EE% of the API up to 91 %. This suggested that a minimal amount of drug was lost during the pressure-spinning process. This loss occurred because some of the drug precipitated inside the pot and, therefore, did not get carried into the fibers. The EE% value reported here exceeds those of a binary polymer system of PCL/PEO prepared by pressure-spinning for the same API, with an EE% of 73 % [48].

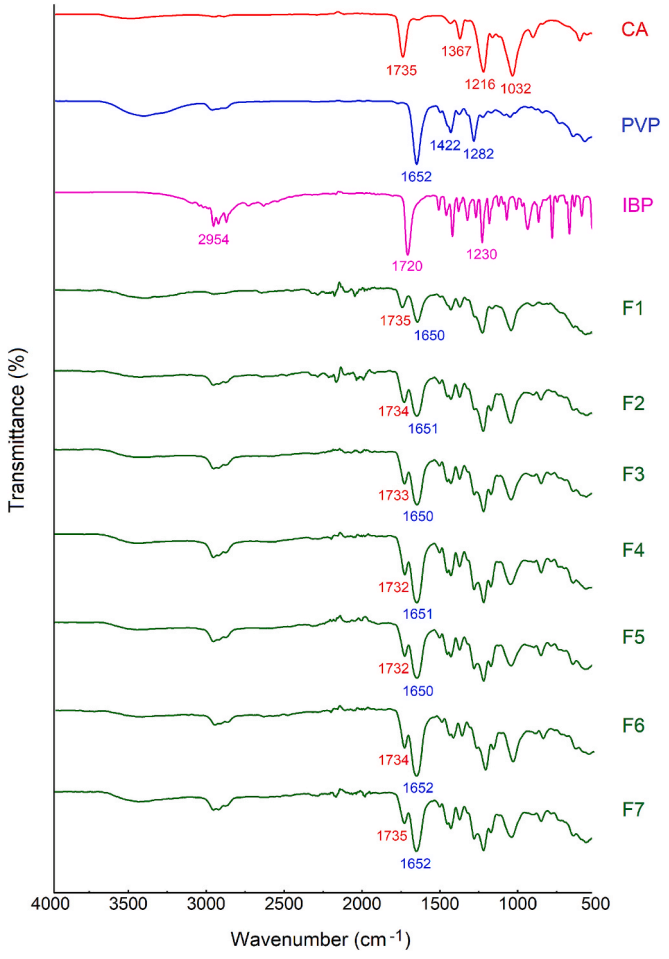

Fig. 8. FTIR spectra of raw materials and IBP-loaded core-sheath pressure-spun fibers.

Table 6
The EE% of IBP in the pressure-spun nanofibers.

Formulation	EE (%, mean ± SD)
F1	91 ± 5
F2	88 ± 1
F3	74 ± 9
F4	84 ± 3
F5	88 ± 2
F6	83 ± 9
F7	90 ± 7

3.9. Dissolution test

The results of the *in vitro* dissolution study are plotted in Fig. 9. The core-sheath nanofibers manufactured were able to perform a biphasic release consisting of a fast release followed by a slow release. 29–42 % of IBP was immediately released from the core-sheath pressure-spun nanofibers after they were placed in the dissolution media for 15 min. This finding suggests that, despite their poor water solubility, IBP molecules can dissolve alongside PVP when the samples are placed in an aqueous medium, facilitating immediate drug release. This occurs due to the application of PVP as a sheath layer material in the matrix. PVP is an especially beneficial polymer for fast-dissolving drug delivery systems due to its high hydrophilicity and rapid solubility in water [11,49]. The utilization of hydrophobic CA as a core material allowed the release of IBP to be maintained over an extended period.

Fig. 9a depicts the release profile of IBP from the optimization of drug concentration in the nanofibers. In the first 15 min, F1, F2, and F3 could release 29 %, 37 %, and 40 % of IBP, respectively. After 12 h of observation, F3, with the highest IBP concentration, released almost all of the drug loaded in the nanofibers (99 %), while the maximum percentage release from F1 and F2 was 75 % and 88 %, respectively. The data suggests that the low-IBP-loaded nanofiber formulations exhibited slower release of the model drug compared to the high-loading formulations. This observation aligns with experimental findings reported by other researchers, who studied a different concentration of IBP loaded into hydrophilic polymeric pressure-spun fibers [50] or hydrophobic polymeric electrospun fibers [51]. This can be explained by the fact that at higher IBP concentrations, a larger amount of the drug is positioned on the surface of the nanofibers, making it more exposed to the surrounding solution [52]. Porosity has been demonstrated to play a pivotal role in accelerating the release of IBP by increasing the surface area and enhancing fluid penetration [53]. As the IBP leaves, it will create pores in the fibers, and there will be more pores with a higher IBP loading. Additionally, the increased IBP content in the nanofiber system may create a significant concentration gradient, thereby enhancing the effective driving force for diffusion [54]. Conversely, at lower IBP concentrations, the drug tends to be predominantly encapsulated within the nanofiber matrix. Furthermore, the slow degradation of the polymer (CA) and the interaction between CA and IBP further hinder the release of IBP [51].

The variation in spinning parameters resulted in the drug release profile depicted in Fig. 9b and 9c. Observation at 15 min showed that 31–45 % of the drug was released from the nanofiber matrix (F4: 39 %, F5: 38 %, F6: 33 %, and F7: 42 %). The nanofibers with the smallest fiber

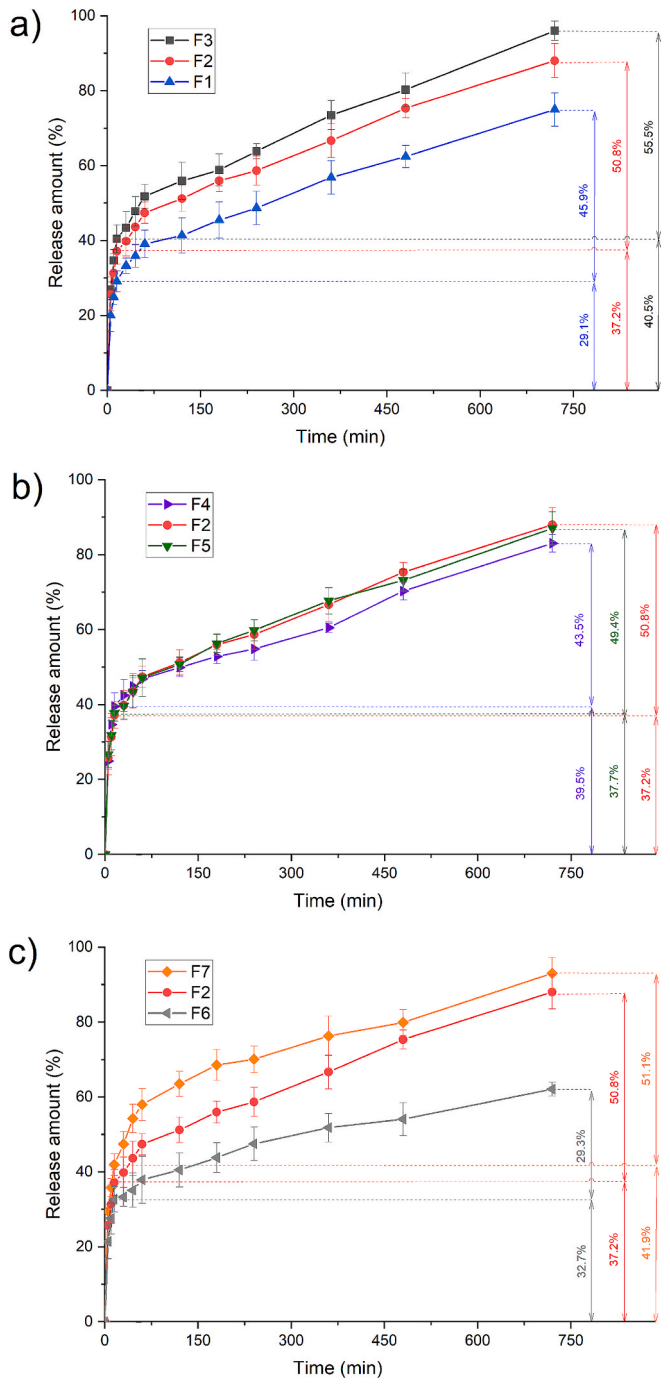

Fig. 9. Release profile comparisons of IBP from core-sheath nanofibers with different: a) drug concentration; b) gas pressure; and c) rotational speed.

diameter, F7, released 93 % of the model drug in 12 h, while F6, the sample with the largest diameter, released only 62 % of IBP in the same time period. This is believed to be due to differences in pressure-spun fiber diameter: as the diameter of the pressure-spun fibers decreased, the released amount of model drug increased, which aligns with findings reported in the literature [22,55,56]. The first possibility is that IBP did not diffuse easily from the interior of the F6 sample due to its larger diameters. The second possibility is that thinner fibers have a much larger surface area relative to their volume than thicker fibers. This increased surface area allows for greater exposure of the fiber material to the surrounding environment and more points of contact for the release of encapsulated substances [56]. The optimization of gas pressure and rotational speed in pressure-spinning allows for the control and adjustment of the release characteristics of the core-sheath nanofiber for the intended application.

3.10. Stability studies

The XRD patterns of the core-sheath nanofibers following an 8-week storage period are presented in Fig. S2. Notably, all patterns exhibited only broad haloes with no discernible sharp peaks. This indicates that the fibers retained their amorphous state after storage. Consistent with these observations, the DSC thermograms of the aged fibers, illustrated in Fig. S3, reveal that no characteristic melting endotherm of IBP was observed after storage, thereby confirming that the aged core-sheath nanofibers underwent no discernible changes in comparison to their fresh counterparts. To assess the functional performance of the aged materials, IBP release profiles for the aged core-sheath nanofibers were acquired and compared with those of the fresh core-sheath nanofibers (Fig. S4). As shown in Fig. S4a, the aged core-sheath pressure-spun nanofiber formulations with varying IBP loading released 73–99 % of their drug loading within 12 h (F1: 73 %; F2: 86 %; and F3: 99 %), exhibiting release profiles that were identical to those observed in the fresh samples. Furthermore, the data in Fig. S4b and c demonstrate that the fibers produced under varying spinning parameters exhibited release patterns ranging from 66 to 90 % over 12 h (F4: 86 %; F5: 90 %; F6: 66 %; and F7: 89 %). The release characteristics observed in the aged samples closely resembled those of the fresh samples, suggesting that the aging process did not adversely affect the release behavior of the drug. This consistency in release profiles indicates that the nanofibers remained stable over time, maintaining their efficacy and functional properties. Overall, these results underscore the potential for using core-sheath pressure-spun nanofibers in drug delivery systems, demonstrating their reliability and durability for prolonged storage.

4. Conclusions

In this study, the CSPS method was successfully employed to manufacture core-sheath structured nanofibers from non-pressure-spinnable CA combined with PVP. Different IBP loading formulations were prepared at 2.5 %, 5 %, and 7.5 %. Additionally, different gas pressure and rotational speed ranging from 0.1-0.3 MPa and 12,000–32,000 RPM, respectively, were also explored. Except for the fibers produced at a low rotational speed, all fibers had a diameter in the nanometer range, with the smallest diameter observed at 370 nm. All the fibers produced were cylindrical and had a smooth morphology on their surface. Confocal microscopy and optical microscope images confirmed the consistent presence of a well-defined core-sheath structure in CA/PVP nanofibers, indicating that the CSPS method effectively produced a two-component architecture, regardless of spinning parameters or drug concentration, underscoring its reliability for manufacturing core-sheath nanofibers. XRD and DSC analyses confirmed that IBP in the core-sheath pressure-spun nanofibers existed in an amorphous state, as indicated by the absence of crystalline Bragg reflections and characteristic IBP melting peaks. The FTIR spectra confirmed the compatibility of materials in the nanofibers, showing characteristic peaks of both PVP and CA, whereas the peak of IBP merged with the C=O bands of the polymers due to hydrogen bonding. The core-sheath pressure-spun nanofibers achieved an EE% of 83–91 % for IBP, with the exception of the sample with a 7.5 % IBP loading, which exhibited an EE% of 74 %. The dissolution tests indicated that the core-sheath nanofibers exhibited biphasic drug release, with 29–42 % of IBP released within the first 15 min due to the fast-dissolving PVP sheath, followed by a slower release maintained by the hydrophobic CA core. Higher IBP concentrations led to faster release, while nanofibers with smaller diameters released a greater percentage of the drug cargo over time due to their larger surface area. The XRD, DSC, and release profile analyses of core-sheath nanofibers after 8 weeks of storage confirmed that the fibers retained their

amorphous state and exhibited similar drug release characteristics, thereby indicating long-term stability. Future research will prioritize optimizing all the key parameters of CSPS in manufacturing core-sheath nanofibers to provide a more comprehensive understanding of the manufacturing of core-sheath pressure-spun fibers.

CRediT authorship contribution statement

Nanang Qosim: Writing – review & editing, Writing – original draft, Visualization, Validation, Methodology, Investigation, Formal analysis, Data curation, Conceptualization. **Gareth R. Williams:** Writing – review & editing, Supervision, Resources, Project administration, Methodology, Conceptualization. **Mohan Edirisinghe:** Writing – review & editing, Supervision, Resources, Project administration, Funding acquisition, Conceptualization.

Declaration of competing interest

The authors declare that they have no known competing financial interests or personal relationships that could have appeared to influence the work reported in this paper.

Acknowledgments

The authors gratefully acknowledge the support of the UK Engineering and Physical Sciences Research Council (EPSRC) for advancing pressure-spinning research at UCL (Grants EP/S016872/1, EP/N034228/1, and EP/L023059/1). NQ expresses gratitude to Lembaga Pengelola Dana Pendidikan (LPDP), The Ministry of Finance, The Republic of Indonesia, for supporting this work.

Appendix A. Supplementary data

Supplementary data to this article can be found online at https://doi.org/10.1016/j.matdes.2025.113939.

Data availability

Data will be made available on request.

References

[1] W. Huang, Z. Jin, Y. Chen, G. Yang, Y. Xu, Preparation, Characterization, and Drug Release of Electrospun Core-Shell Structured Hyaluronic Acid-Bovine Serum Albumin/Poly (ε-Caprolactone) Nanofiber Membranes, J. Appl. Polym. Sci. (2025) e56794.
[2] N. Padilla-Manzano, S.n. Santander, T. Vera, E. Jara, L.F. Álvarez, B.n. Díaz, R. Bacchiega, J.C. Forero Oliveros, P. Santana, E. Hamm, Combined Effect of the Core–Shell Structure and Variable Wettability in Polymer Fiber Membranes for Dual and Delayed Release of Active Agents, ACS Appl, Polym. Mater. 6 (17) (2024) 10436–10451.
[3] N. Qosim, H. Majd, S. Huo, M. Edirisinghe, G.R. Williams, Hydrophilic and hydrophobic drug release from core (polyvinylpyrrolidone)-sheath (ethyl cellulose) pressure-spun fibers, Int. J. Pharm. 654 (2024) 123972.
[4] R. Kurpanik, B. Kolesińska, A. Lechowska-Liszka, K. Sokołowski, A. Ścisłowska-Czarnecka, A. Tarbuk, R. Zielińska, Ł. Zych, E. Stodolak-Zych, Preparation and characterization of peptide-modified core-shell fibrous substrates with UV-blocking properties for corneal regeneration applications, Mater. Des. 245 (2024) 113285.
[5] F. Sangsefidi, M. Salehi, M. Mohammadi, M. Zandi, M.S. Pedram, M. Pezeshki-Modaress, Core/shell nanofibrous conduit containing natural surfactant enhanced axonal regrowth guiding for peripheral nerve regeneration, Mater. Des. 241 (2024) 112955.
[6] Y. Zhu, B. Dai, S. Zhang, J. Liu, S. Xu, W. Liu, X. Chen, H. Zhang, Q. Li, F.O.S. Pang, Tissue Mimetic Membranes for Healing Augmentation of Tendon–Bone Interface in Rotator Cuff Repair, Adv. Mater. 2407358 (2025).
[7] V. Thukral, N. Qosim, A. Kurniawan, M. Gültekinoğlu, H.T.U. Herath, G. R. Williams, M. Edirisinghe, Manufacturing and Biological Potential of Saliva-Loaded Core-Sheath Pressure-Spun Polymeric Fibers, Macromol. Mater. Eng. 2400403 (2025).
[8] T. Ju, J. Li, A. Weston, G. Satta, S. Bolognini, M. Di Luca, S. Gaisford, G. R. Williams, Anti-Pseudomonas Aeruginosa Bacteriophage Loaded Electrospun Fibers for Antibacterial Wound Dressings, Macromol. Rapid Commun. 2400744 (2025).
[9] A.H. Saleh, A.M. Badr, Z.A. Muhammad, M.E. Zaki, A.E. Abdelkader, N.A. Mahana, A.S.A. Dena, Tea-Tree Oil-Loaded Core–Shell Chitosan/Polycaprolactone Nanoparticles: In-Vitro Cytotoxicity, Anti-Inflammatory, and Antimicrobial Activities, BioNanoScience 15 (1) (2025) 1–11.
[10] L. Xu, H. He, Y. Du, S. Zhang, D.-G. Yu, P. Liu, Electrosprayed core (cellulose acetate)–shell (polyvinylpyrrolidone) nanoparticles for smart acetaminophen delivery, Pharmaceutics 15 (9) (2023) 2314.
[11] G.R. Williams, B.T. Raimi-Abraham, C. Luo, Nanofibres in drug delivery, UCL Press, 2018.
[12] B. Pant, M. Park, S.-J. Park, Drug delivery applications of core-sheath nanofibers prepared by coaxial electrospinning: a review, Pharmaceutics 11 (7) (2019) 305.
[13] Z. Aytac, T. Uyar, Applications of core-shell nanofibers: Drug and biomolecules release and gene therapy, Elsevier, Core-shell nanostructures for drug delivery and theranostics, 2018, pp. 375–404.
[14] M.F. Abdullah, T. Nuge, A. Andriyana, B.C. Ang, F. Muhamad, Core–shell fibers: Design, roles, and controllable release strategies in tissue engineering and drug delivery, Polymers 11 (12) (2019) 2008.
[15] N. Qosim, Y. Dai, G.R. Williams, M. Edirisinghe, Structure, properties, forming, and applications of alginate fibers: A review, Int. Mater. Rev. 09506608241280419 (2024).
[16] Y. Dai, J. Ahmed, M. Edirisinghe, Pressurized Gyration: Fundamentals, Advancements, and Future, Macromol. Mater. Eng. 2300033 (2023).
[17] S. Mahalingam, S. Homer-Vanniasinkam, M. Edirisinghe, Novel pressurised gyration device for making core-sheath polymer fibres, Mater. Des. 178 (2019) 107846.
[18] S. Mahalingam, S. Huo, S. Homer-Vanniasinkam, M. Edirisinghe, Generation of core–sheath polymer nanofibers by pressurised gyration, Polymers 12 (8) (2020) 1709.
[19] H. Alenezi, M.E. Cam, M. Edirisinghe, Core–sheath polymer nanofiber formation by the simultaneous application of rotation and pressure in a novel purpose-designed vessel, Appl. Phys. Rev. 8 (4) (2021).
[20] H. Majd, M. Gultekinoglu, C. Bayram, B. Karaosmanoğlu, E.Z. Taşkıran, D. Kart, Ö. D. Erol, A. Harker, M. Edirisinghe, Biomedical Efficacy of Garlic-Extract-Loaded Core-Sheath Plasters for Natural Antimicrobial Wound Care, Macromol. Mater. Eng. 2400014 (2024).
[21] S. Mahalingam, C. Bayram, M. Gultekinoglu, K. Ulubayram, S. Homer-Vanniasinkam, M. Edirisinghe, Co-Axial Gyro-Spinning of PCL/PVA/HA Core-Sheath Fibrous Scaffolds for Bone Tissue Engineering, Macromol. Biosci. 21 (10) (2021) 2100177.
[22] H. Majd, A. Harker, M. Edirisinghe, M. Parhizkar, Optimised release of tetracycline hydrochloride from core-sheath fibres produced by pressurised gyration, J. Drug Deliv. Sci. Technol. 72 (2022) 103359.
[23] N. Qosim, H. Majd, J. Ahmed, G. Williams, M. Edirisinghe, Making fibers from cellulose derivatives by pressurized gyration and electrospinning, Cellul. (2024) 1–18.
[24] Y. Yang, W. Li, D.-G. Yu, G. Wang, G.R. Williams, Z. Zhang, Tunable drug release from nanofibers coated with blank cellulose acetate layers fabricated using tri-axial electrospinning, Carbohydr. Polym. 203 (2019) 228–237.
[25] M. Wang, R. Ge, P. Zhao, G.R. Williams, D.-G. Yu, S.A. Bligh, Exploring wettability difference-driven wetting by utilizing electrospun chimeric Janus microfiber comprising cellulose acetate and polyvinylpyrrolidone, Mater. Des. 226 (2023) 111652.
[26] Z.U. Arif, The Role of Polysaccharide-based Biodegradable Soft Polymers in the Healthcare Sector, Adv. Ind. Eng. Polym. Res. (2024).
[27] D. Edikresnha, T. Suciati, M.M. Munir, K. Khairurrijal, Polyvinylpyrrolidone/cellulose acetate electrospun composite nanofibres loaded by glycerine and garlic extract with in vitro antibacterial activity and release behaviour test, RSC Adv. 9 (45) (2019) 26351–26363.
[28] D.-G. Yu, J.-H. Yu, L. Chen, G.R. Williams, X. Wang, Modified coaxial electrospinning for the preparation of high-quality ketoprofen-loaded cellulose acetate nanofibers, Carbohydr. Polym. 90 (2) (2012) 1016–1023.
[29] M. Kurakula, G.K. Rao, Pharmaceutical assessment of polyvinylpyrrolidone (PVP): As excipient from conventional to controlled delivery systems with a spotlight on COVID-19 inhibition, J. Drug Deliv. Sci. Technol. 60 (2020) 102046.
[30] D. Li, M. Wang, W.-L. Song, D.-G. Yu, S.W.A. Bligh, Electrospun Janus beads-on-a-string structures for different types of controlled release profiles of double drugs, Biomol. 11 (5) (2021) 635.
[31] H. He, M. Wu, J. Zhu, Y. Yang, R. Ge, D.-G. Yu, Engineered spindles of little molecules around electrospun nanofibers for biphasic drug release, Adv. Fiber Mater. (2021) 1–13.
[32] Y. Liu, P. Zhou, Z. Cao, W. Liang, J. Yan, H. Xu, L. Wu, L. Sun, L. Gong, C. Peng, Simultaneous solubilization and extended release of insoluble drug as payload in highly soluble particles of γ-cyclodextrin metal-organic frameworks, Int. J. Pharm. 619 (2022) 121685.
[33] J. Zhou, P. Wang, D.-G. Yu, Y. Zhu, Biphasic drug release from electrospun structures, Expert Opin. Drug Deliv. 20 (5) (2023) 621–640.
[34] X. Zheng, S. Kang, K. Wang, Y. Yang, D.-G. Yu, F. Wan, G.R. Williams, S.-W.-A. Bligh, Combination of structure-performance and shape-performance relationships for better biphasic release in electrospun Janus fibers, Int. J. Pharm. 596 (2021) 120203.
[35] E. Latiffah, A. Sawitri, B.H. Agung, D.A. Hapidin, D. Edikresnha, E. Elfahmi, K. Khairurrijal, Antibacterial activity of electrospun nanofibers polyvinylpyrrolidone/cellulose acetate matrix loaded by Ageratum conyzoides L. weed, Case Stud. Chem, Environ. Eng. 9 (2024) 100651.

[36] W.X. Waresindo, H.R. Luthfianti, D. Edikresnha, T. Suciati, F.A. Noor, K. Khairurrijal, A freeze–thaw PVA hydrogel loaded with guava leaf extract: Physical and antibacterial properties, RSC Adv. 11 (48) (2021) 30156–30171.
[37] S. Mahalingam, M. Edirisinghe, Forming of polymer nanofibers by a pressurised gyration process, Macromol. Rapid Commun. 34 (14) (2013) 1134–1139.
[38] A. Kelly, J. Ahmed, M. Edirisinghe, Manufacturing Cyclodextrin Fibers Using Water, Macromol. Mater. Eng. 307 (6) (2022) 2100891.
[39] X. Hong, S. Mahalingam, M. Edirisinghe, Simultaneous application of pressure-infusion-gyration to generate polymeric nanofibers, Macromol. Mater. Eng. 302 (6) (2017) 1600564.
[40] E.S. Medeiros, G.M. Glenn, A.P. Klamczynski, W.J. Orts, L.H. Mattoso, Solution blow spinning: A new method to produce micro-and nanofibers from polymer solutions, J. Appl. Polym. Sci. 113 (4) (2009) 2322–2330.
[41] P.L. Heseltine, J. Ahmed, M. Edirisinghe, Developments in pressurized gyration for the mass production of polymeric fibers, Macromol. Mater. Eng. 303 (9) (2018) 1800218.
[42] J. Gu, S. Yagi, J. Meng, Y. Dong, C. Qian, D. Zhao, A. Kumar, T. Xu, A. Lucchetti, H. Xu, High-efficiency production of core-sheath nanofiber membrane via co-axial electro-centrifugal spinning for controlled drug release, J. Membr. Sci. 654 (2022) 120571.
[43] J. Jauhari, S. Wiranata, A. Rahma, Z. Nawawi, I. Sriyanti, Polyvinylpyrrolidone/cellulose acetate nanofibers synthesized using electrospinning method and their characteristics, Mater. Res. Express 6 (6) (2019) 064002.
[44] L.-M. Her, S.L. Nail, Measurement of glass transition temperatures of freeze-concentrated solutes by differential scanning calorimetry, Pharm. Res. 11 (1994) 54–59.
[45] W. Li, D.-G. Yu, K. Chen, G. Wang, G.R. Williams, Smooth preparation of ibuprofen/zein microcomposites using an epoxy-coated electrospraying head, Mater. Lett. 93 (2013) 125–128.
[46] A.W. Jatoi, I.S. Kim, Q.-Q. Ni, Cellulose acetate nanofibers embedded with AgNPs anchored TiO2 nanoparticles for long term excellent antibacterial applications, Carbohydr. Polym. 207 (2019) 640–649.
[47] L. Wei, J. Song, B. Cheng, Z. Yang, Synthesis, characterization and antibacterial properties of novel cellulose acetate sorbate, Carbohydr. Polym. 243 (2020) 116416.
[48] A. Afshar, H. Majd, A. Harker, M. Edirisinghe, Tailored binary polymer system PCL-PEO for advanced biomedical applications: Optimization, characterization and in vitro analysis, J. Drug Deliv. Sci. Technol. 95 (2024) 105582.
[49] C. Li, Z.-H. Wang, D.-G. Yu, G.R. Williams, Tunable biphasic drug release from ethyl cellulose nanofibers fabricated using a modified coaxial electrospinning process, Nanoscale Res. Lett. 9 (2014) 1–10.
[50] B.T. Raimi-Abraham, S. Mahalingam, P.J. Davies, M. Edirisinghe, D.Q. Craig, Development and characterization of amorphous nanofiber drug dispersions prepared using pressurized gyration, Mol. Pharmaceutics 12 (11) (2015) 3851–3861.
[51] C. Sun, L. Zou, Y. Xu, Y. Wang, Ibuprofen-loaded poly (lactic acid) electrospun mats: The morphology, physicochemical performance, and in vitro drug release behavior, Macromol. Mater. Eng. 305 (12) (2020) 2000457.
[52] Y. Geng, G.R. Williams, Developing and scaling up captopril-loaded electrospun ethyl cellulose fibers for sustained-release floating drug delivery, Int. J. Pharm. 648 (2023) 123557.
[53] X. Chen, H. Li, W. Lu, Y. Guo, Antibacterial porous coaxial drug-carrying nanofibers for sustained drug-releasing applications, Nanomaterials 11 (5) (2021) 1316.
[54] P. Pankongadisak, S. Sangklin, P. Chuysinuan, O. Suwantong, P. Supaphol, The use of electrospun curcumin-loaded poly (L-lactic acid) fiber mats as wound dressing materials, J. Drug Deliv. Sci. Technol. 53 (2019) 101121.
[55] Y. Geng, F. Zhou, G.R. Williams, Developing and scaling up fast-dissolving electrospun formulations based on poly (vinylpyrrolidone) and ketoprofen, J. Drug Deliv. Sci. Technol. 61 (2021) 102138.
[56] S. Chen, X. Huang, X. Cai, J. Lu, J. Yuan, J. Shen, The influence of fiber diameter of electrospun poly (lactic acid) on drug delivery, Fibers Polym. 13 (2012) 1120–1125.